Pure & Appl. Chem., Vol. 58, No. 12, pp. 1647–1656, 1986.
Printed in Great Britain.

Transport phenomena in ultrafiltration: membrane selectivity and boundary layer phenomena

Gunnar Jonsson

Instituttet for Kemiindustri, Technical University of Denmark, DK 2800 Lyngby, Denmark

Abstract - Retention characteristics of UF membranes are delineated through comparison of the combined viscous flow and frictional model with the Ferry-Faxen equation. The molecular weight cut-off concept is discussed using calculations of how sharp cut-off curves one can expect of UF membranes with uniform pore sizes and how heteroporosity will affect such curves. Experimental retention-flux curves for different macromolecules have been measured. From these data the molecular weight cut-off curves at varying pressure levels can be determined and by comparing with the model an average pore radius can be calculated.

Permeate flux is often more or less pressure independent, which has been explained by a gel layer formation at the membrane surface. However, recently it has been shown that for many types of macromolecules it is rather an osmotic pressure of the concentrated boundary layer, which is responsible for the special flux-pressure relationship.

INTRODUCTION

The selectivity of ultrafiltration membranes is determined primarily by the ratio between the hydrodynamic diameter of the solute and the apparent pore diameter. Thus the retention characteristics of a given membrane are usually presented as the retention versus the molecular weight of different macromolecules. The molecular weight cut-off is said to be that M_w-value which is almost totally rejected. However, for most UF membranes the retention-molecular weight curve is not very sharp, indicating a relatively heteroporous membrane structure. Also, factors such as the shape and dissociation of the macromolecules influence the retention.

Most ultrafiltration data are so highly influenced by the concentration polarization that a determination of the membrane transport properties is very uncertain. Often, one finds that the flux is independent of pressure and that the retention decreases with pressure (ref. 1), which is inconsistent with all transport theories that consider only the membrane. However, if the membrane system design is such that a correction for the concentration polarization can be calculated, models for transport within the membrane can be validated.

THEORETICAL MOLECULAR WEIGHT CUT-OFF CURVES

In an earlier paper (ref. 2) different methods for determining the selectivity of reverse osmosis membranes were investigated. A combined viscous flow and frictional model was found to give the best correlation with the experimental data. This so-called finely-porous model has been presented in detail (ref. 3). It was shown to give a good description of retention data for rather tight UF membranes having M_w cut-off values in the range 1000-6000 daltons.

According to this model the true membrane retention is given by the relation:

$$\frac{c_m}{c_p} = \frac{1}{1-R} = \frac{b}{K} + \left(1 - \frac{b}{K}\right) \exp\left(- \frac{t\lambda}{\varepsilon} \frac{J_v}{D_i}\right) \qquad (1)$$

Here b is a friction factor and K is the distribution coefficient of solute between pore fluid and bulk solution. The "effective skin layer thickness",

$t\lambda/\varepsilon$, is a membrane parameter which should be independent of the solute used. The pore distribution coefficient and the friction parameter were correlated with the Ferry-Faxen equation (refs. 4,5) in the following way:

$$K = \frac{(A_i/A_p)_{steric}}{(A_w/A_p)_{steric}} \tag{2}$$

and

$$b = \frac{(A_w/A_p)_{friction}}{(A_i/A_p)_{friction}} \tag{3}$$

where

$$(A_i/A_p)_{steric} = 2(1-\alpha)^2 - (1-\alpha)^4 \tag{4}$$

and

$$(A_i/A_p)_{friction} = 1 - 2.104\ \alpha + 2.09\ \alpha^3 - 0.95\ \alpha^5 \tag{5}$$

Here $\alpha = d_i/d_p$ is the ratio between the solute diameter to the pore diameter. When a value of 46 Å was used for the pore diameter, the experimentally determined K and b values were in reasonable agreement with Eqs. (2-5).

The effect of heteroporosity on the retention–solute size curve

From Eq. (1) the maximum retention corresponding to $J_v \to \infty$ is given by:

$$R_{max} = 1 - \frac{K}{b} \tag{6}$$

Using Eqs. (2-6) it is possible to calculate the maximum retention as a function of solute diameter for different pore diameters. Figure 1 shows the calculated R_{max}-values versus the logarithm of the hydrodynamic solute diameter for three different pore diameters: 50, 100 and 150 Å, respectively. For a heteroporous membrane with a mean pore diameter of 100 Å consisting of two pore sizes - 50 and 150 Å - in such a ratio that the permeate flux through the small pores is the same as through the larger pores, it can be shown that the mean R_{max}-value, $\bar{R}_{max}$, is given by:

$$(\bar{R}_{max})_{100} = \frac{1}{2}\left((R_{max})_{50} + (R_{max})_{150}\right) \tag{7}$$

This is represented by the dotted line shown in Fig. 1. Comparing this average curve with the curve for $d_p = 100$ Å in the same figure, we can see that the quite broad selectivity curves for ultrafiltration membranes could be due to the transport mechanism rather than to the variation in pore sizes of the membranes. Thus a very steep selectivity curve cannot be expected even for ultrafiltration membranes with uniform pore sizes.

The effect of pressure on the retention–solute size curve

Figure 1 only shows the variation with solute size on the intrinsic membrane properties, represented by R_{max}. In practice, however, the observed retention normally changes with variation in pressure. This is caused by the increase in flux with pressure, thereby increasing the real retention given by Eq. (1). In addition, the concentration polarization, c_m/c_b, which can be calculated from the film model:

$$\frac{c_m - c_p}{c_b - c_p} = \exp\left(J_v \frac{\delta}{D_i}\right) \tag{8}$$

also increases with flux. This reduces the observed retention, S, which is the parameter of interest for the practical separation process.

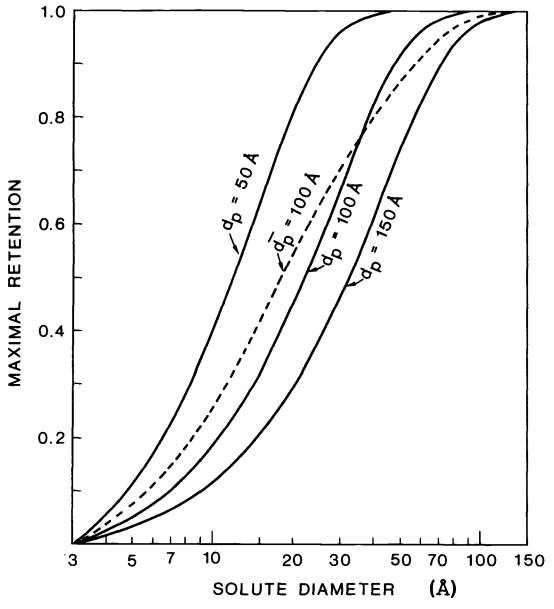

Fig. 1. The maximal retention, R_{max}, calculated from Eqs. (2-6) versus the solute diameter. The dotted curve represents a heteroporous membrane calculated from Eq. (7) (ref. 7).

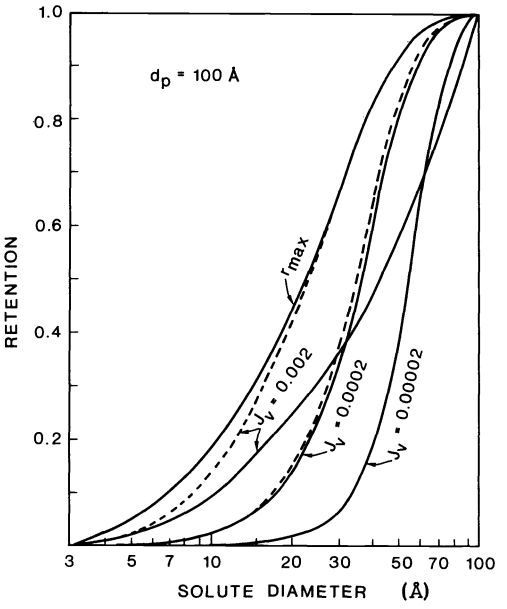

Fig. 2. Retention versus solute diameter for three different values of the permeate flux. The dotted curves are the real membrane retention calculated from Eq. (1). The solid curves are the observed retentions, where the concentration polarization calculated from Eq. (8) is further taken into account (ref. 7).

Using Eqs. (2-5) together with Eqs. (1) and (8) it is possible to calculate the real membrane retention, $R = 1-c_p/c_m$ and the observed retention, $S = 1 - c_p/c_b$, when D_i, $t\lambda/\varepsilon$ and δ are known. Here, the diffusion coefficient in the external solution is calculated from the Stokes-Einstein equation:

$$D_i = \frac{kT}{3 \pi \eta d_i} \qquad (9)$$

while $t\lambda/\varepsilon$ and δ are assumed equal to 30 μm and 10 μm, respectively. These are normal values for ultrafiltration membranes (ref. 3) and ultrafiltration systems working at high circulation velocities (ref. 6).

Figure 2 shows the calculated retentions for three different levels of permeate flux: 2×10^{-3}, 2×10^{-4} and 2×10^{-5} cm/s, which corresponds to a high, low and extremely low ultrafiltration flux, respectively. The dotted curves are calculated from Eq. (1) only, without taking the concentration polarization from Eq. (8) into account. At high flux (2×10^{-3} cm/s) Eq. (1) gives R-values that are quite close to the maximal retention. But the concentration polarization increases drastically with increasing solute diameter, so that the observed retention is much smaller than R_{max}. With or without concentration polarization the cut-off curve is quite broad, indicating that sharp solute-solute separation is not possible at high flux levels. In addition, gel formation and fouling are often observed even at low bulk concentrations, which further complicate any solute separation. At low flux (2×10^{-4} cm/s), Eq. (1) gives R-values that are much lower than R_{max}, especially for low and medium retaining solutes. As the concentration polarization is quite low for all solute sizes this gives a quite steep cut-off curve. Therefore, solute separation should be much better at low pressures. At extremely low flux (2×10^{-5} cm/s), there is no concentration polarization and the cut-off curve is even steeper: however, the flux is so low that it is not economically feasible.

EXPERIMENTAL MOLECULAR WEIGHT CUT-OFF CURVES

Recently, Jonsson and Christensen (Ref. 8) measured retention-flux curves for a series of polyethyleneglycols (PEG) and dextrans, from which the molecular weight cut-off curves at varying pressure levels were determined.

Figures 3 and 4 show the observed retention versus the permeate flux for three PEG's and dextrans, respectively. Due to polarization the curves go through a maximum at which point the increase in true retention is balanced by the increase in concentration polarization. The flux value where the maximum is situated depends mainly on the retention level and the mass transfer coefficient. This special phenomenon may result in such a situation that the observed retention of a larger molecule will be lower than that of a smaller molecule. This is seen in Fig. 3, where the curves for PEG 20,000 and PEG 6,000 cross each other at high flux values. In Figs. 3 and 4 the real membrane retention calculated from Eq. (8) using experimentally determined values for the mass transfer coefficient, $k = D_i/\delta$, are further shown as dotted curves. Now a steady increase in retention is seen approaching the maximal retention at infinite flux.

Figure 5 shows the elution curves for a mixture of PEG standards and a dextran T 10, respectively. In addition, the permeate from a dextran T 10 solution is shown as the dotted curve. From comparison with the elution curve for the bulk solution, a clear shift to a lower molecular weight can be seen. Figure 6 shows two similar comparisons of the bulk and permeate solution for PEG 20,000

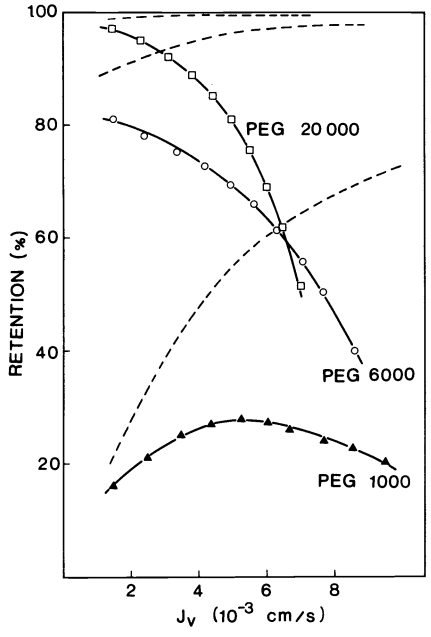

Fig. 3. Observed retention versus permeate flux for three different PEGs. The dotted curves are the true membrane retention calculated from Eq. (8)

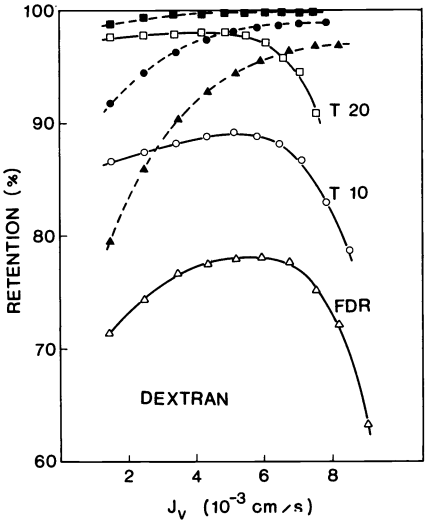

Fig. 4. Observed retention versus permeate flux for three different dextrans. The dotted curves are the true membrane retention calculated from Eq. (8) (ref. 8).

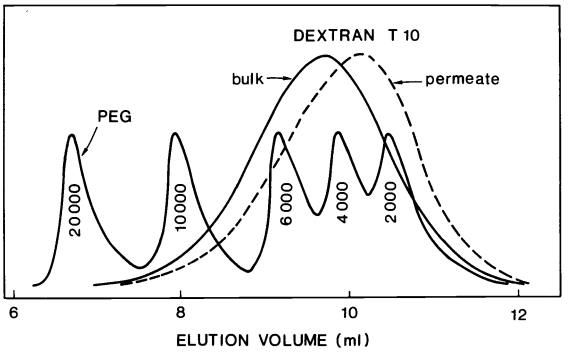

Fig. 5. Elution curves for a mixture of PEG standards. Further a comparison of the bulk and permeate for dextran T 10 (ref. 8).

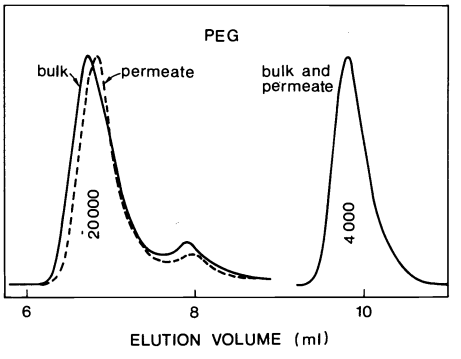

Fig. 6. Comparison of the bulk and permeate for PEG 20,000 and PEG 4,000 (ref. 8).

and PEG 4,000, respectively. For the high molecular weight solute a shift is again seen, whereas the low molecular solute is unchanged. The elution curve for PEG 20,000 shows further that there is some impurity of PEG 10,000 in this substance. Comparing the top heights of the concentrated permeate and the bulk solution it can be seen that PEG 10,000 is decreased in concentration relative to PEG 20,000. This is in agreement with the situation shown in Fig. 3, where the retention of PEG 20,000 falls below that of PEG 6,000 at high pressure. From the calibration curves for PEG and dextran it is found that M_w is reduced from 20,000 to 18,500 for PEG 20,000 and from 9,300 to 6,300 for dextran T 10 by the permeation through the membrane.

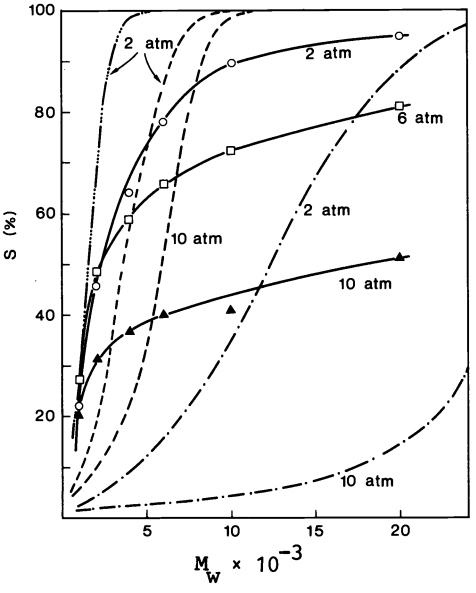

Fig. 7. Observed retention versus molecular weight for PEG at three different pressure levels. The dotted curves are calculated from Eqs. (1-4) and (8-10) for three different pore radii: r_p = 20 Å (-...-), r_p = 30 Å (---) and r_p = 60 Å (-·-) (ref. 8).

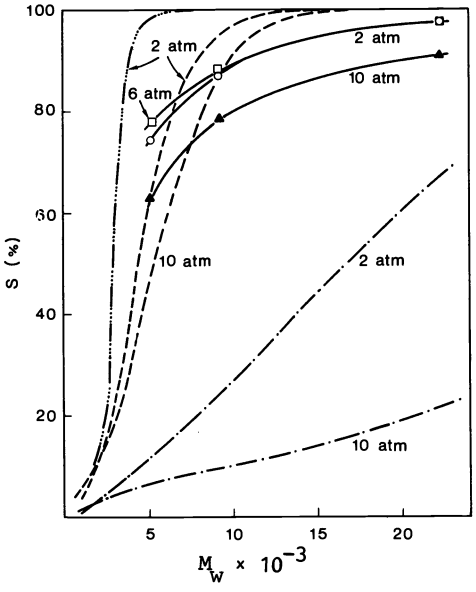

Fig. 8. Observed retention versus molecular weight for dextran at three different pressure levels. The dotted curves are calculated from Eqs. (1-4) and (8-10) for three different pore radii: r_p = 20 Å (-···-), r_p = 30 Å (---) and r_p = 60 Å (-·-) (ref. 8).

Figures 7 and 8 show cut-off curves at three different pressure levels for PEG and dextran, respectively. At low pressure the retention level for the two different macromolecules is quite similar, but with increasing pressure the retention for PEG decreases strongly, whereas dextran shows a maximum at 6 atm and then decreases a little. This different behaviour seems mainly to be caused by a difference in the solution properties of the two macromolecules. PEG has a higher hydrodynamic volume than dextran at the same molecular weight and so a lower diffusivity. Therefore concentration polarization is more severe for PEG than for dextran while the retention decreases much faster. This phenomenon is verified in Fig. 9, where the cut-off curve is given as the intrinsic value, R_{max}, versus M_w. Here PEG, dextran and polyvinylpyrro-

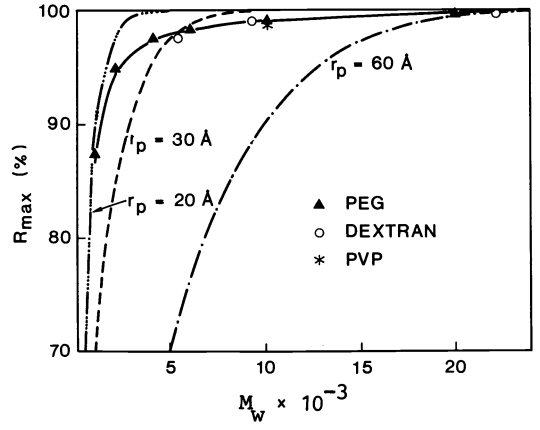

Fig. 9. The maximal retention determined from Eq. (1) versus molecular weight for all the macromolecules investigated. The dotted curves are calculated from Eqs. (2-4) and (10) for three different pore radii (ref. 8).

lidon (PVP) fall on almost the same curve, showing that the separation characteristics of the membrane itself are primarily determined by the molecular weight of the solute. The maximal retention, R_{max}, was estimated from the finely porous model, Eq. (1), by determining the two parameters b/K and $t\lambda/\varepsilon$ using a non-linear parameter estimation for the calculated values of R versus J_v shown as the dotted curves in Figs. 3 and 4.

The retention data were further correlated with the equations for steric exclusion and frictional interaction with the pore walls as given by Eqs. (2-6). Instead of using Eq. (5) we used a slightly modified equation given by Haberman and Sayre (ref. 9):

$$(A_i/A_p)_{friction} = \frac{1-2.105\ \alpha + 2.0865\ \alpha^3 - 1.7068\ \alpha^5 + 0.72603\ \alpha^6}{1-0.75857\ \alpha^5} \quad (10)$$

In Fig. 9, $R_{max} = 1-K/b$ has been calculated for PEG for three different pore radii and shown as a function of M_w determined from literature values. At low M_w the experimental data are close to the curve for r_p = 20 Å, but above M_w = 2,000 they increase much slower than expected from Eqs. (2-4) and (10). At M_w = 5,000 they cross the curve for r_p = 30 Å, approaching the curve for r_p = 60 Å at M_w = 20,000, where R_{max} is close to unity. This may indicate that the membrane has an average pore radius around 30 Å, but a pore size distribution from 20 Å to 60 Å with quite few pores in the upper range.

In Figs. 7 and 8 similar curves have been calculated for the observed retention in the following way: From Eqs. (2-4) and (10) the parameter b/K is calculated for different r_i and r_p values. Then the true retention, R, is calculated from Eq. (1) at different pressure levels (corresponding to given J_v-values) assuming $t\lambda/\varepsilon = 10^{-4}$ cm and D_i determined from Eq. (9). Finally, the observed retention is calculated from Eq. (8) knowing the mass transfer coefficient at the recirculation velocity u = 250 cm/s, and M_w from the literature. Again, for M_w <2,000 the experimental data are quite close to the calculated curve for r_p = 20 Å. At M_w = 5,000 the experimental data at 2 and 10 atm cross the calculated curves for r_p = 30 Å and they seem to approach the 60 Å curve for M_w-values above 20,000. Thus the similarity in the position of the calculated curves relative to the experimental data in Figs. 7 and 9 seems to confirm that the membrane has a pore size distribution between 20 Å and 60 Å for r_p.

BOUNDARY LAYER PHENOMENA

Polarization phenomena at the membrane-solution interface are usually characterized by the film-theory model, in which longitudinal mass transport within the boundary layer is assumed negligible (ref. 10). In the ultrafiltration of macromolecular solutions, it has generally been observed that as pressure is increased, permeate flux first increases and then remains more or less pressure independent. This phenomenon was first explained by Blatt et al. (ref. 1) who argued that the reason for the observed pressure independence was due to the formation of a gel layer at the membrane surface. By increasing the pressure above a certain limit, a temporary flux increase results in an accumulation of gel at the membrane surface. Steady state is attained when the hydraulic resistance of the gel layer has decreased the permeate flux to the limiting value:

$$(J_v)_{lim} = \frac{\Delta P}{R_m + (t_g/P_g)} = k \times \ln \frac{c_g}{c_b} \quad (11)$$

Thus the limiting flux increases with decreasing bulk concentration, c_b, and increasing mass transfer coefficient, k. Although the gel model has shown great utility, the assumption about a gel layer with well-defined gel concentration, c_g, and variable thickness, t_g, determined by the pressure difference across the gel layer is not generally acceptable.

Wales (ref. 11) argues that for most lyophilic systems it is not likely there exists a pressure gradient across the polarization layer. Only for such

materials as agar, pectin, gelatin, and some proteins, which might be denatured at the membrane surface to give true gels, it would be expected to find gel-controlled polarization layers. One of the reasons for ignoring the osmotic pressure in Eq. (11) is that by using the Van't Hoff equation for calculating the osmotic pressures, these are negligible as compared to the hydraulic pressure. In the past,osmotic pressure measurements of macromolecular solutions have generally been confined to the dilute range and have been taken primarily for the purpose of obtaining molecular weights and conformational data. Only in few instances measurements have been made up to moderate concentrations. Neither are existing theoretical models of highly nonideal solution behavior suitable for a priori prediction at high concentrations.

Recently, Jonsson (ref. 12) determined experimentally the osmotic pressure of concentrated solutions of dextran and whey protein. Above 20 wt% of the macromolecules, the osmotic pressure increased very steeply. The concentration dependence of the osmotic pressure could be expressed by a third virial expansion:

$$\Pi = A_1 C + A_2 C^2 + A_3 C^3 \qquad (12)$$

In Fig. 10 the osmotic pressure and viscosity of dextran T10 are shown as a function of concentration. It can be seen that a 50 wt% dextran solution is still Newtonian with a quite low viscosity (η = 2.7 Poise) compared to the very high osmotic pressure (Π = 25.5 atm). Therefore it seems unlikely that the gel model can explain what really happens in the ultrafiltration process.

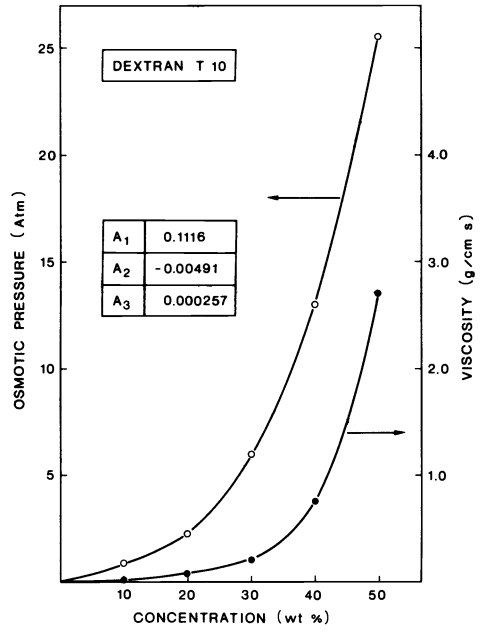

Fig. 10. Osmotic pressure and viscosity data for dextran T10 at varying concentrations. The curve for the osmotic pressure has been calculated from Eq. (12) using the statistically determined values for the virial coefficients (ref. 12).

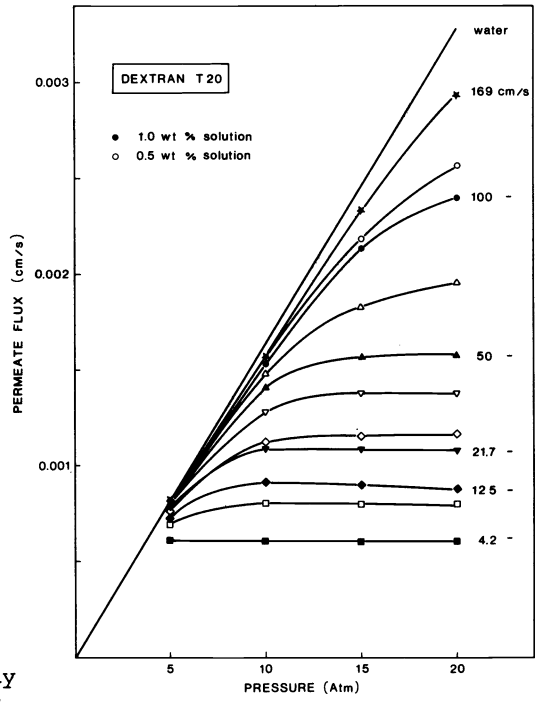

Fig. 11. Flux-pressure relationships for dextran T20 solutions at two concentration levels and varying velocities (ref. 12).

UF data of dextran and whey proteins

In an earlier investigation at our institute (ref. 13) permeate flux was measured versus pressure for dextran T20 and Whey Pro-90 at varying concentrations and circulation velocities. Figure 11 shows the data for dextran T20, where the circulation velocity is varied from 169 cm/s to 4.2 cm/s at two concentration levels. Below 50 cm/s the permeate flux becomes constant or slightly decreasing at high pressures indicating that a gel layer is formed on the membrane surface. However, in the literature (ref. 1) most data with dextrans show that the gel concentration should be about 35 wt%, which seems unreasonably low as compared with the data in Fig. 10. Assuming the levelling

TABLE 1. Calculated values of the mass transfer coefficient, k (10^{-5}cm/s), as a function of concentration, c_b, and pressure, ΔP, using Eqs. (8) and (12-13), and the experimental data in Fig. 11.

c_b	ΔP	Circulation velocity, u (cm/s)					
(wt%)	(atm)	169	100	50	21.7	12.5	4.2
1.0	10	101	74	52	34	28	18
1.0	15	110	73	47	31	25	17
1.0	20	100	71	44	29	24	16
0.5	10	-	68	48	35	29	20
0.5	15	-	62	47	33	27	19
0.5	20	-	65	46	32	27	18

off in permeate flux is not caused by a real gel layer, but rather by an osmotic pressure of the concentrated boundary layer, it is possible to calculate the osmotic pressure at the membrane surface, Π_m, from the relation:

$$J_v = l_p (\Delta P - \Pi_m) \quad (13)$$

where l_p is determined from the slope of the pure water flux. The concentration at the membrane surface, c_m, can then be calculated from Eq. (12), assuming that the osmotic pressure of dextran T20 is the same as that of dextran T10. This is probably a reasonable assumption at higher concentrations, where the osmotic pressure is less dependent on molecular weight than on the total mass of macromolecules (ref. 14). Knowing c_m it is possible to calculate the mass transfer coefficient, $k = D_i/\delta$, from the film model, Eq. (8).

In Table 1 the calculated values of k are given. This shows that at a given circulation velocity, k seems reasonably constant although there is a slight tendency that k decreases with increasing pressure and concentration. This is not surprising since the viscosity increases and the diffusivity decreases with increasing concentration, which both give a decrease in k. This also explains why the permeate flux can even decrease with pressure: increasing the pressure from 10 to 20 atm for the 1% solution at 12.5 cm/s, the concentration at the membrane surface increases from 26.9 wt% to 41.4 wt% assuming k constant. At the same time the osmotic pressure increases from 4.5 to 14.2 atm giving a rise in the driving force by only 0.3 atm. However, if k decreases slightly as indicated in Table 1, c_m increases instead to 41.6% which has an osmotic pressure of 14.7 atm so that the driving force now decreases by 0.2 atm and therefore the permeate flux must decrease too!

In Fig. 12 some UF data on whey protein are shown. Permeate flux was measured versus pressure with the bulk concentration increasing from 0.1 to 9.1 wt%. All data were taken at u = 100 cm/s. Again the permeate flux becomes constant or slightly decreasing at high pressures for concentrations above 4.8 wt%. Using the measured osmotic pressure data it is possible to calculate the permeate flux-pressure curve for a given value of k: From Eq. (8) c_m is calculated for fixed values of J_v and c_b. Using Eq. (12) Π_m is calculated and finally ΔP is calculated from Eq. (13). The solid curves in Fig. 12 are calculated in this way using a constant value of 0.00040 cm/s for the mass transfer coefficient. As seen this gives a quite good correlation with the experimental data. Especially when taking into account that the water permeability changed somewhat under the experiments why the water curve from which l_p is calculated is an average one. As also seen in Fig. 11 and Table 1 it seems that the mass transfer coefficient decreases slightly with increasing pressure. However, it gives a very good correlation with the decrease in permeate flux with increasing concentration.

One of the strongest arguments for the gel model is that one normally finds a linear relation between the permeate flux and the logarithm to the bulk concentration (ref. 15). This should intercept the x-axis ($J_v = 0$) at the gel concentration according to Eq. (11). Using typical values of k and l_p from Fig. 11 and Table 1, the permeate flux for dextran solutions at increasing bulk concentration has been calculated at constant pressure (ΔP = 10 atm): From Eq. (13) Π_m is calculated at a fixed value of J_v. Then c_m is calculated from

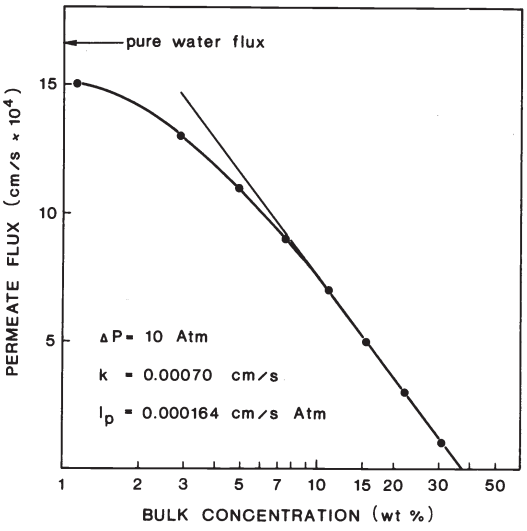

Fig. 13. Calculated values of J_v versus log (c_b) for dextran T10 at constant pressure using Eqs. (8) and (12-13) (ref. 12).

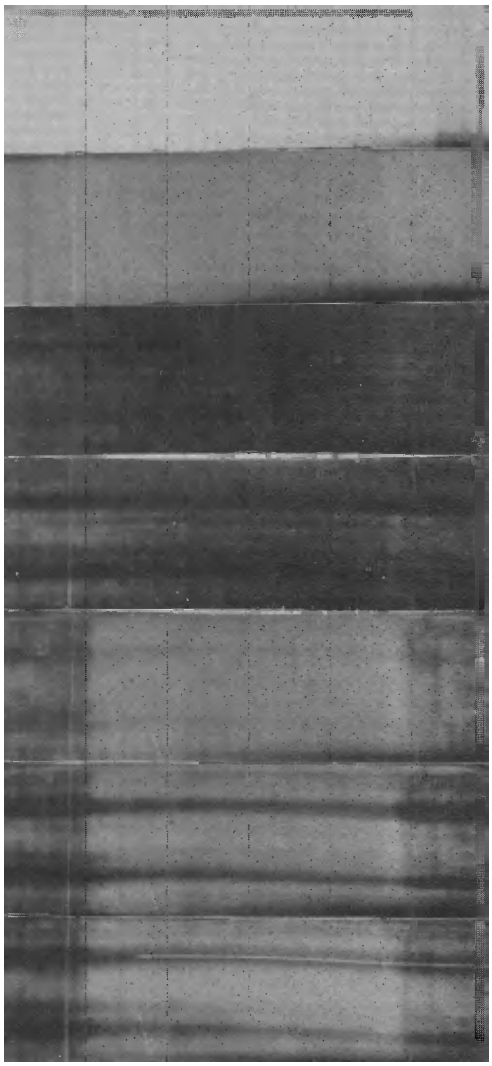

(a) water

(b) u = 17 cm/s
ΔP ≈ 0 atm

(c) u ≈ 0 cm/s
ΔP = 10 atm

(d) u = 8 cm/s
ΔP = 10 atm

(e) u ≈ 0 cm/s
ΔP = 10 atm

(f) u = 8 cm/s
ΔP = 10 atm

(g) u = 8 cm/s
ΔP = 10 atm

Fig. 14. Pictures of the membrane surface taken under ultrafiltration conditions with 1% iron dextran solution at varying pressure and circulation velocities. The flow direction is from left to right. In pictures (e)-(g) part of the membrane surface was reduced in permeability to 10% of the original permeability. In the last picture a hole was punched in the membrane surface.

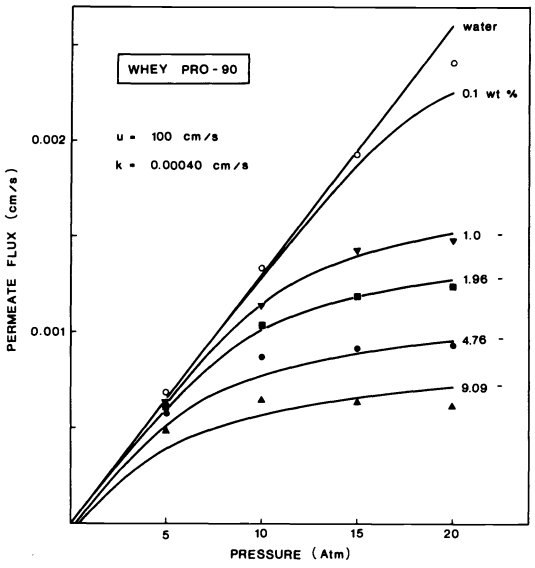

Fig. 12. Flux-pressure relationships for whey protein solutions at varying concentrations, but constant circulation velocity. The curves have been calculated from Eqs. (8) and (12-13) using a constant value for the mass transfer coefficient (ref. 12).

Eq. (12) and finally c_b from Eq. (8). Figure 13 shows the calculated values in a semilogarithmic plot of J_v versus log (c_b). As seen this gives a linear relation at bulk concentrations above 7 wt%, intersecting the x-axis at a "gel concentration" of about 37 wt%. However, from Fig. 10 this "gel" has a viscosity below 50 cP but an osmotic pressure of 10 atm. Using Eq. 11 the mass transfer coefficient can be calculated from the slope of the line in Fig. 13. This gives a value of 0.00058 cm/s which is only 17% lower than the value used for the calculations in Fig. 13. Thus the gel model fits reasonably well with the calculated data; however, it is not the gel concentration which is determined from the intercept with $J_v = 0$, but the concentration at which the solution has an osmotic pressure equal to the applied pressure!

Evidence for a moving boundary layer

In the gel layer model, Eq. (11), it is assumed that all transport within the boundary layer is perpendicular to the membrane surface. However, recent observations with colored macromolecules (ref. 12) show that transport is rather three-dimensional: Besides the back diffusion of the macromolecules from the membrane surface to the bulk solution, the concentrated boundary layer was accumulated in certain areas, possibly due to secondary currents perpendicular to the flow direction and then moving along the flow direction showing thin stripes on the membrane surface.

Figure 14 shows some pictures of the membrane surface taken through an acrylic window in a special thin channel test cell during ultrafiltration of a 1% iron dextran solution. The channel dimensions were: 47 cm (length), 2.5 cm (width) and 0.08 cm (height). The membrane had the same dimension as the flow channel, but was divided into 10 equally large permeate outlets in series. The window shows the membrane surface in the far end of the channel (length = 36.2 to 43.7 cm).

Picture (a) in Fig. 14 shows the white surface of the polysulphone membrane with water in the system. Picture (b) shows the same membrane surface when a 1% iron dextran solution is circulated at very low pressure in the system. In picture (c) the pressure was slowly increased from 0 to 10 atm within 75 seconds. In this period the pressure accumulator was filled with solution so that the test cell worked as a dead end cell ($u \sim 0$ cm/s). This gives an almost even distribution of concentrated iron dextran solution. When the back pressure valve opens for the circulation at 10 atm, the pattern shown in picture (d) is obtained within a minute ($u = 8$ cm/s).

Pictures (e) and (f) show some situations in which the membrane piece above permeate outlet number 9 had been swabbed with acetone so that the water permeability decreased to about 10% of the original. Pictures (e) and (f) correspond to the situations shown in pictures (c) and (d), respectively, before the swabbing of the membrane. This clearly shows that the appearance of the stripes has something to do with the hydrodynamics of the flowing solution. Also it shows that within the stripes the concentrated boundary layer is flowing along the membrane surface in the channel direction. This is even more clearly shown in picture (g) where a very tiny hole was punched in the membrane

surface at the position where it was known that the broad stripe appeared at u = 8 cm/s. The concentrated boundary layer is skimmed off through the hole leaving a yellow stripe of bulk solution behind. Obviously mixing within the stripe is extremely low. Even though the flux from permeate outlet number 9 only increased with about 10% it was enriched in iron dextran concentration to about 1.3 wt%. Therefore the concentration of the solution flowing through the hole must be in the range 10-20 wt%.

LIST OF SYMBOLS

A_i	area available for transport of solute
b	friction parameter
c	concentration of solute
d_i	solute diameter
d_p	pore diameter
D_i	diffusion coefficient
J_v	volume flux
k	mass transfer coefficient
K	distribution coefficient of solute between pore fluid and bulk solution
l_p	hydraulic permeability
ΔP	pressure difference
P_g	permeability of gel layer
R	retention of solute
R_m	membrane resistance
t	tortuosity factor
t_g	thickness of gel layer
T	temperature
α	ratio between solute diameter and pore diameter
δ	polarization layer thickness
ε	fractional pore area
η	viscosity
λ	membrane thickness
Π	osmotic pressure

Subscripts

b	bulk solution
g	gel layer
i	solute
m	at membrane surface
p	permeate
w	water

REFERENCES

1. W.F. Blatt, A. Dravid, A.S. Mickaels and L. Nelsen, in "Membrane Science and Technology" 47-97, J.E. Flinn (ed.) Plenum Press, New York (1970).
2. G. Jonsson, Desalination 24, 19-37 (1978).
3. G. Jonsson and C.E. Boesen, Desalination 17, 145-165 (1975).
4. J.D. Ferry, J. Gen. Physiol. 20, 95 (1936).
5. H. Faxen, Ark. Mat. Astron Fysik 17, 27 (1922).
6. G. Jonsson and C.E. Boesen, Desalination 21, 1-10 (1977).
7. G. Jonsson, Desalination 53, 3-10 (1985).
8. G. Jonsson and P.M. Christensen, in "Membranes and Membrane Processes" 179-190, E. Drioli (ed.), Plenum Press, New York (1986).
9. W.L. Haberman and R.M. Sayre, "Motion of Rigid and Fluid Spheres in Stationary and Moving Liquids Inside Cylindrical Tubes", David Taylor Model Basin Report. No. 1143. Department of the Navy (1958).
10. G. Jonsson and C.E. Boesen, in "Synthetic Membrane Processes" 101-130, G. Belfort (ed.), Academic Press, New York (1984).
11. M. Wales, in "Synthetic Membranes: Desalination 159-170, A.F. Turbak (ed.), American Chemical Society, Washington, D.C. (1981).
12. G. Jonsson, Desalination 51, 61-77 (1984).
13. L.J. Jørgensen, M.Sc. Thesis, Instituttet for Kemiindustri (1979).
14. P.J. Flory, Principles of Polymer Chemistry, Cornell University Press, Ithaca, NY (1953).
15. M.C. Porter, Ind. Eng. Chem. Prod. Res. Develop. 11 234-248 (1972).